High-gradient *C*-band linac for a compact x-ray free-electron laser facility

T. Inagaki,* C. Kondo, H. Maesaka, T. Ohshima, Y. Otake, T. Sakurai, K. Shirasawa,† and T. Shintake†

RIKEN SPring-8 Center, Kouto 1-1-1, Sayo, Hyogo, 679-5148, Japan

(Received 7 April 2014; published 7 August 2014)

An electron linac using a *C*-band rf frequency, 5.712 GHz, has enabled us to obtain an acceleration gradient of more than 35 MV/m reliably. A *C*-band accelerator system has been developed and constructed for the compact x-ray FEL facility, SACLA, in order to fit within the available site length at SPring-8, and to reduce construction costs. An accelerator unit consists of two 1.8 m-long accelerator structures, a cavity-type rf pulse compressor and a 50 MW pulsed klystron. In order to achieve a compact rf source and to obtain extremely stable rf fields in the accelerator structures, an oil-filled, high-voltage pulse modulator combined with an extremely stable, inverter-type, high voltage charger was developed. SACLA uses 64 sets of these accelerator units in order to achieve a final beam energy of 8.5 GeV. After rf conditioning for 1 700 hours, the maximum acceleration gradient achieved was 38 MV/m. The typical trip rate for each accelerator unit at 35 MV/m and 30 pps is about once per day. Dark current from the accelerator structures is less than 5 pC, which causes a negligible effect on the beam monitors. The phase and amplitude stability of the rf fields were measured to be 0.03 degree and 0.01% rms, respectively, which is sufficient for the XFEL operation of SACLA. Since the first beam commissioning in 2011, the *C*-band accelerator has demonstrated fairly stable performance under continuous operation for 20 000 hours.

DOI: 10.1103/PhysRevSTAB.17.080702 PACS numbers: 29.20.Ej, 41.60.Cr, 84.70.+p

I. INTRODUCTION

The x-ray free-electron laser (XFEL) is a fourth-generation light source, which provides ultrabrilliant, highly coherent, femtosecond x-ray pulses to many frontier experiments. The XFEL radiation is generated by extremely high-dense, high-energy electron beams that pass through a long undulator after being accelerated in a linac. The photon energy is inversely proportional to undulator period, and is proportional to the square of the electron beam energy. Since a permanent-magnet undulator period is practically limited to about 18 mm to obtain sufficient magnetic field, a beam energy of about 8 GeV is necessary to generate 10 keV or higher photon energies. In the world's first XFEL facility, the Linac Coherent Light Source (LCLS) [1] at SLAC, one-third of the existing *S*-band linac was reused to accelerate an electron beam up to 14 GeV, with an acceleration gradient of about 17 MV/m. However, such a long linac with a long facility building would have been difficult to realize as a brand-new XFEL facility, because of the high construction costs. Instead, a compact linac with a higher acceleration gradient is used to make the cost manageable.

The acceleration gradient of a linac with constant-gradient, traveling-wave-type rf structures is

$$E_{\mathrm{acc}} = \sqrt{\frac{P_{in} \cdot R_{sh} \cdot (1 - e^{-2\tau})}{L}},$$

where P_{in}, R_{sh}, τ, and L are the input rf power, the shunt impedance per unit length, attenuation parameter and the active structure length, respectively. According to the frequency scaling laws of rf structures [2], the shunt impedance, R_{sh}, is proportional to $f^{0.5}$, where f is the rf frequency. The group velocity of the traveling-wave rf structure is proportional to $f^{1.5}$. Assuming the structure length L and attenuation parameter τ are fixed, the rf structure fill time decreases as $f^{-1.5}$ with increasing frequency. If the pulsed power from an rf source is fixed, the shorter pulse length allows us to obtain higher peak power, P_{in}, by using an rf pulse compression technique, such as SLAC's energy doubler, SLED [3]. For these reasons, the acceleration gradient is roughly proportional to its operating rf frequency. Indeed, since the 1990's, new high-gradient linacs with *C*-band (5.7 GHz) [4] and X-band (11.4 GHz) [5] rf frequencies have been proposed for high-energy physics experiments, instead of the conventional S-band (2.8–3.0 GHz) linacs.

However, there are gradient limits at which rf structures can operate reliably. The practical upper limit of the surface field in a standard copper cavity is around 100 MV/m due

*inagaki@spring8.or.jp

†Present address: Okinawa Institute of Science and Technology Graduate University, Tancha 1919-1, Onna-son Kinigami-gun, Okinawa 904-0495, Japan.

to rf breakdown, dark current and surface heating [6]. Since the peak surface field is about 2 or 3 times higher than the acceleration gradient, the surface field of our *C*-band structures is around this upper limit, while the surface field in X-band rf structures reaches up to 150–200 MV/m.

Another difficulty in the higher frequency bands is the precise machining accuracy required for the rf cells. In the case of the *C*-band accelerator structure, the tolerance on the cell diameter is about 1 μm in order to realize a total phase advance error within 10 degrees. The tolerances of the X-band cells is even tighter because of its higher frequency, although cell tuning is typically used to loosen the tolerances.

A strong single-bunch transverse wakefield effect due to the small disk apertures of the rf structure is also a problem for the higher frequency bands. According to the short-range wakefield model of Ref. [7], the transverse wake is roughly proportional to $a^{-3.5}$, where a is the aperture radius. Since a quite low-emittance and high peak-current electron beam is required for the XFEL, all of the aperture positions in the accelerator structure should be well aligned with the electron beam axis to make the transverse wakefield small. For our linac, the alignment tolerances for the *C*-band rf structures are about 0.3 mm, which are achievable by existing fabrication and alignment methods.

The availability of a high-power rf source is also an important factor in the linac design. Development of the *C*-band accelerator system, including a high-power pulsed klystron, was originally started for a e^+e^- linear collider project [4,8] in the 1990's. When our XFEL project was proposed in 2001 [9], a 50-MW class *C*-band (5.712 GHz) klystron was commercially available.

For these reasons, a *C*-band frequency linac was considered the most suitable for a compact XFEL facility to obtain a high acceleration gradient reliably and to have manageable alignment tolerances. The Japanese XFEL facility called the SPring-8 Angstrom compact free-electron laser (SACLA) [10] chose a *C*-band accelerator system. In this report, we first briefly introduce SACLA and the *C*-band accelerator system, followed by important components in the system: the acceleration structure, the SLED system and the modulator. Finally, the operational performance of the *C*-band accelerator is discussed.

II. DESIGN OF THE *C*-BAND LINAC

A. Configuration of SACLA

SACLA employs a 5 to 8.5 GeV electron beam to generate x rays with sub-mJ pulse energies and 5 to 20 keV photon energies. The total length of the SACLA facility is 700 m, which is limited by the available space at the SPring-8 campus. The compact facility also allows a reduction of the construction costs, which was realized by three key technologies: a high-gradient *C*-band linac, a low-emittance thermionic electron, and a short-period in-vacuum undulator.

Figure 1 shows the configuration of the SACLA accelerator. A 500 kV-pulsed thermionic electron gun with a CeB_6 single crystal cathode generates a stable, low-emittance, high-current, single-bunch-per-pulse electron beam [11]. The beam is longitudinally compressed by a velocity bunching process in successive 238 and 476 MHz subharmonic bunchers, which are standing-wave cavities. Subsequently, the beam is also compressed by three magnetic bunch compressors: BC1, BC2 and BC3, each consisting of a four bend magnetic chicane, in order to obtain a final peak current of 3 kA [12]. The energy chirps for the compression stages are given by off-crest rf acceleration in *L*-band (1.428 GHz) APS-type standing-wave structures before BC1, *S*-band (2.856 GHz) traveling-wave accelerator structures before BC2 and *C*-band (5.712 GHz) traveling-wave accelerator structures before BC3. These accelerator frequencies were chosen to minimize the nonlinear energy variation along the bunches to achieve optimal compression. After BC3, the electron beam is accelerated up to the final energy by running on-crest in *C*-band accelerators. The *C*-band linac consists of an array of "accelerator units," each including a klystron and accelerator structures as described in a later section. In addition, a quadrupole magnet, a steering magnet, electron beam monitors [13] and a gate valve were installed between every four accelerator units, which are grouped as a "section." In the SACLA linac, 12 accelerator units (section CB01-CB03) are used from BC2 to BC3, and 52 units (section CB05-CB18) are used after BC3.

B. Linac requirements

The *C*-band linac as the main accelerator of SACLA should satisfy the following requirements: (i) The electric

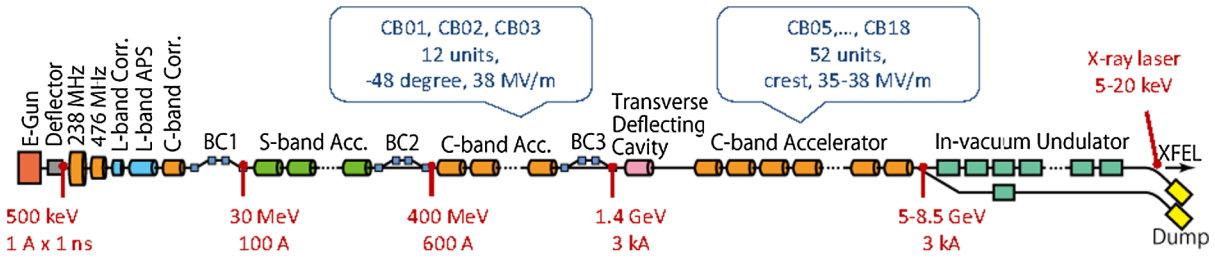

FIG. 1. Schematic of the SACLA accelerator, and the typical operation parameters for the electron beam and the *C*-band accelerator units. CB01, CB02,… are the names of the *C*-band accelerator sections, which consist of four accelerator units.

field gradient of the accelerator structures needs be about 38 MV/m to achieve an electron beam energy of 8.5 GeV within the prescribed linac length. (ii) The trip (interlocked stop) rate of each accelerator unit should be less than once per 24 hours. SACLA has about 70 accelerator units. If one of the accelerator units trips, the electron beam is shut off for about one minute until the rf power is restored and the rf stabilized. This is done to avoid beam loss in the undulator sections. In order to reduce the loss in beam operation time to less than 5%, the trip rate of the SACLA linac should be less than once every 20 minutes. (iii) The dark current, emitted from the inner surfaces of the accelerator structures, should be much less than the bunch charge of 300 pC per pulse. Some part of the dark current will be captured and accelerated, which generates a noise signal in the electron beam monitors. In addition, the dark current may cause radiation damage to the machine components, in particular, demagnetization of the undulators. (iv) Since the high-acceleration gradient shortens the total length of the linac, klystrons and klystron modulators should be compact in order to fit longitudinally along the klystron gallery. (v) For stable generation of the x rays, the amplitude and phase of the rf field in the accelerator structure should be extremely stable. The reason is that the electron peak current after the bunch compression process is quite sensitive to the energy chirp along a bunch given by the upstream accelerators [12]. For example, the rms tolerances of the rf pulse-to-pulse fluctuations for the *C*-band accelerators upstream of BC3 is 0.01% in amplitude and 0.2 degrees in phase. We have designed and developed the *C*-band accelerator system to satisfy the above requirements.

C. *C*-band accelerator unit configuration

Figures 2 and 3 show the configuration of the *C*-band accelerator unit. In order to obtain a high acceleration gradient, 50 MW pulsed klystrons [8] are used to supply high rf power to two traveling-wave accelerator structures after rf pulse compression by a SLED-type rf pulse compressor. Under nominal operation, the output power of the klystrons are designed to be about 40 MW, which is 80% of the maximum value of 50 MW, providing a safety margin and long-term reliability. Using SLED, the rf pulse width is compressed from 2.5 to 0.5 μs to multiply the average rf power during the output pulse by roughly 4 times. The rf power is fed into two quasi-constant-gradient accelerator structures, which are 1.8 m long each, generating an acceleration gradient of up to 38 MV/m. Thus, the beam energy gain of a 4 m-long *C*-band accelerator unit is about 136 MeV. The waveguide size for the *C*-band unit is WR-187. Its upper usable frequency of 6.0 GHz is close to the operational rf frequency, which leads to a low power loss and a low surface electrical field. The total power loss

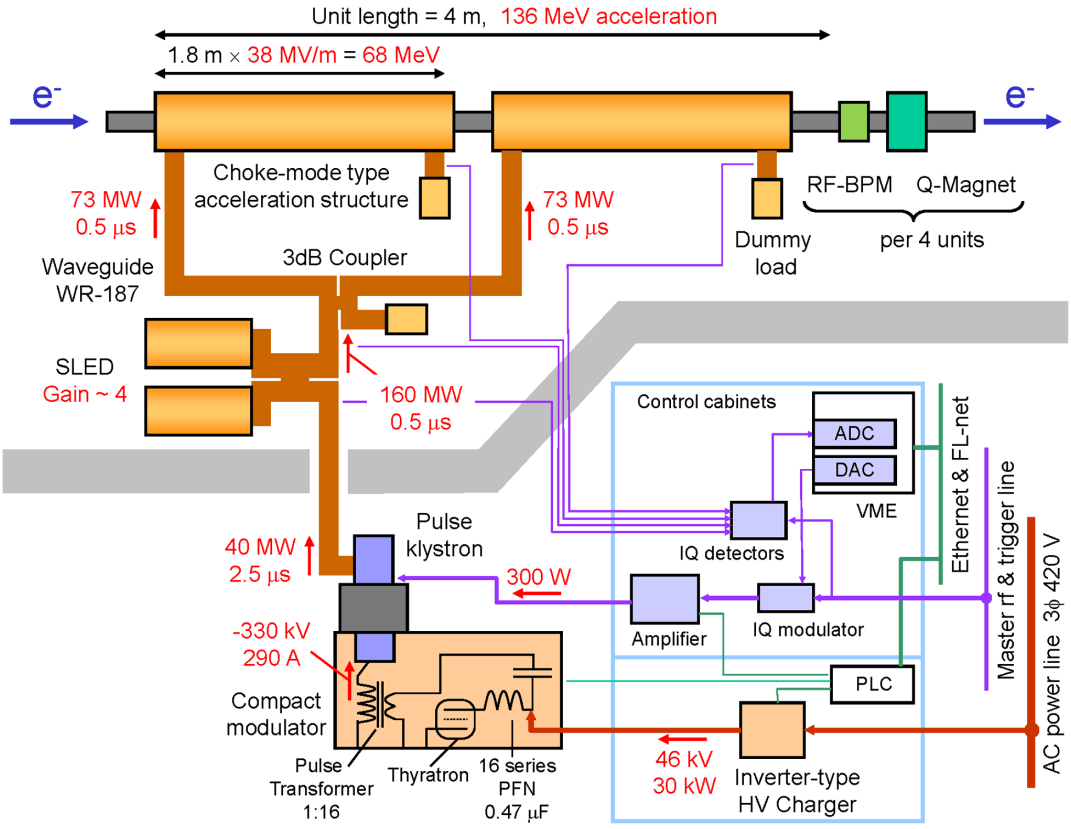

FIG. 2. Configuration of the *C*-band accelerator unit. Typical parameters for nominal operation are given in the figure.

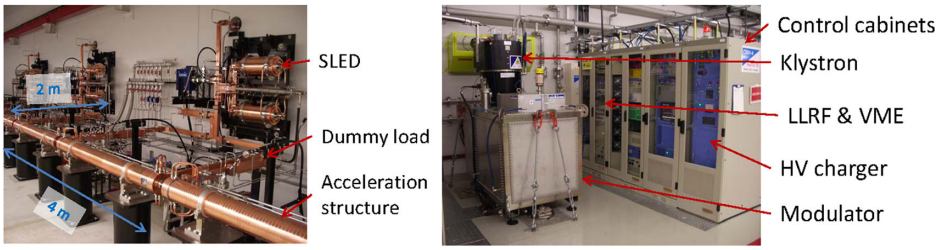

FIG. 3. Photograph inside the accelerator tunnel (left figure) and that of the klystron gallery (right figure) of the SACLA *C*-band accelerator.

between the klystron and the accelerator structures is about 10%, including the Ohmic loss on the inner waveguide surfaces and the contact resistances of the waveguide flanges. At the downstream structure ports, the rf power is absorbed in silicon-carbide (SiC) rf loads. The rf power from the klystrons, SLED systems and the downstream structure ports are monitored via rf directional couplers. In order to operate at high rf fields, the vacuum pressure of the accelerator structures, SLED cavities and waveguide components are kept below 10^{-6} Pa by five sputter-ion pumps attached to the waveguides. We use a pair of rf ceramic windows at the klystron's dual output port, and no additional rf windows between the klystrons and the accelerator structures, because the rf windows are not reliable with 50 MW rf power transmission.

In order to install a klystron and modulator every 4 m to match the accelerator length, we developed a compact oil-filled modulator combined with an inverter-type high-voltage charger. Their sizes, compared to the conventional open-air type modulators, was drastically reduced. The klystrons, modulators and control enclosures for the *C*-band accelerator unit are alternately placed along the klystron gallery. The modulator includes a line-type pulse-forming network (PFN) circuit, a thyratron tube as a high-voltage switch and a pulse transformer in a steel tank. The voltage variation of the PFN circuit is one of the largest sources of rf phase and amplitude variation. The voltage regulation of our high-voltage charger was improved substantially to satisfy the rf stability requirement of 0.01% in amplitude.

The rf drive power for the klystron is supplied by a 500 W solid-state amplifier. In order to stabilize the rf power from the klystron, it is operated in saturation mode. Radio-frequency pulse modulation and phase and amplitude control are realized by an in-phase and quadrature (IQ) modulation of the low-level rf (LLRF) signal [14]. The LLRF system also includes several sets of IQ detectors combined with 12-bit or 16-bit ADC modules, which measure the rf amplitude and phase at the klystron output, the SLED output, and the accelerator structure downstream port. The rf phases measured with the IQ detector are kept at target values by feedback control using the IQ modulators and detectors, which are controlled by a VERSA-module Europe bus (VME) computer. In order to avoid phase drift due to surrounding temperature changes, the LLRF system and the solid-state amplifier were enclosed in a water-cooled 19-inch cabinet.

The temperature stability of the cooling water in the SACLA utility system is about ± 0.2 C. This cooling water stabilizes the temperature of the klystrons, modulators, control cabinets and the solid-state amplifiers. Since the rf phases in the accelerator structures and in the SLED systems are quite sensitive to changes in temperature, a precise temperature control system was introduced for these devices [15]. The system regulates the water temperature to within ± 0.02 C, which corresponds to an rf phase stability of ± 0.2 degree for the accelerator structures and ± 0.3 degree for the SLED output.

All of these components are connected to a PLC-based local control system and VME modules located in each control cabinet. They are remotely controlled and monitored from the control room via the MADOCA framework [16]. Manual control by operators or automatic control sequences set various parameters for each unit, such as the charging voltage, rf phase, pulse timing and repetition rate. This control system allows us to operate with much flexibility. In order to recover quickly from various machine faults, several "standby" units are operated at a timing of 10 μs before the nominal beam-arrival time. If a certain problem occurs in one of the "in-service" units, an operator can easily switch the standby and in-service units so as to recover the beam acceleration.

D. Accelerator structures

Figure 4 shows the cross-sectional view of the accelerator structure used in SACLA. Its parameters are summarized in Table I. In order to effectively obtain a high acceleration efficiency, a traveling-wave structure with a quasiconstant gradient was chosen. A unique feature of the structure is its "choke-mode" cell geometry [17]. This feature was included for multibunch operation in a future upgrade. At the outer diameter of each cell, an rf choke structure is used to prevent leakage of the acceleration rf mode, while a coaxial SiC rf-power absorber effectively damps the transmitted higher-order rf modes (HOM), and so suppresses the long-range wakefield effect with multi-bunched beams. To provide more room for the choke joints,

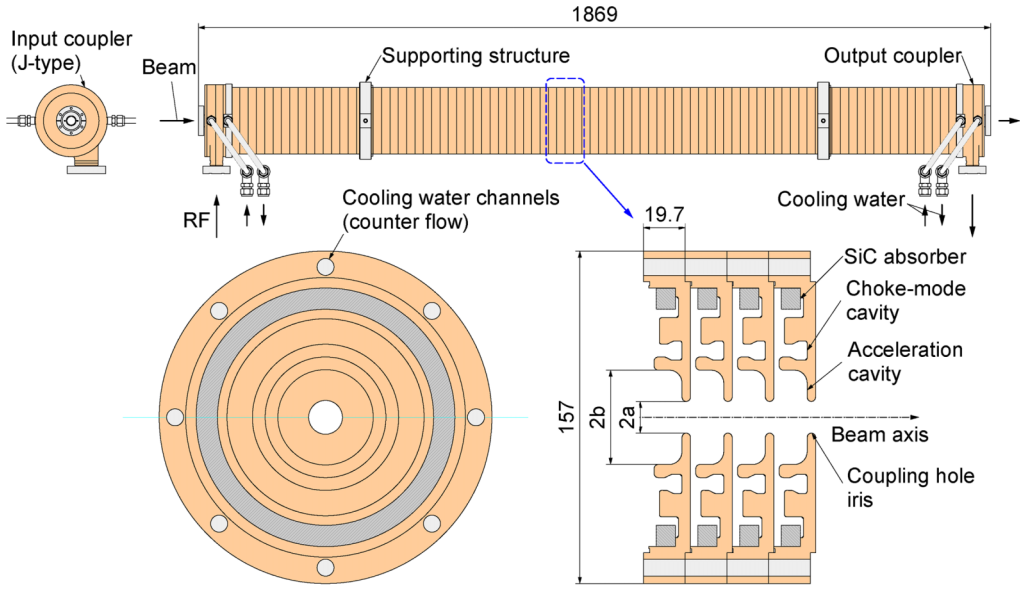

FIG. 4. Top view (top) and the cross sectional view (bottom) of the *C*-band choke-mode accelerator structure.

the $3\pi/4$ rf fundamental mode was selected, which has a 2.2 mm longer cell length than conventional $2\pi/3$ mode cells. Ninety-one cavity cells, including input and output coupler cells, are assembled into a 1.8 m-long column. The iris aperture diameters and the shunt impedances of the cells are shown in Fig. 5. In order to compensate the power attenuation along the structure, the aperture diameter is linearly tapered so as to obtain a quasiconstant acceleration gradient as shown in Fig. 5. Each edge of the coupling-hole iris between the cells is rounded with a curvature radius of 2 mm so as to reduce the surface electrical field to less than 100 MV/m. The input and output couplers are the *J*-type, double-fed style [18]. This coupler design is used to reduce the rf field strength around the edge of the coupling irises between the coupler cell and the waveguide, and to provide a better electromagnetic symmetry in order to reduce any orbital kick effect by the electromagnetic fields [19].

The cavity cells were fabricated from high-purity, oxygen-free copper treated by a hot isostatic pressing (HIP) process. This treatment eliminates residual small voids in the copper material to prevent outgassing from the surface and emission of dark current [20]. Each cell was carefully machined on a high-precision lathe in order to precisely adjust the cavity frequency and to achieve a mirrorlike surface finish for high-voltage durability and low dark-current emission. The cells were vertically stacked and brazed in a vacuum electrical furnace.

TABLE I. *C*-band structure parameters.

Structure type	Traveling wave, quasiconstant gradient
Phase advance per cell	$3\pi/4$
Active accelerator length	1.79 m
Number of cells	91 cells (including two coupler cells)
Cell length	19.7 mm
Iris aperture (2a)	13.6–17.3 mm
Iris thickness	4 mm
Accelerator cavity diameter (2b)	44.0–45.7 mm
Operating frequency	5712 ± 0.2 MHz
Average phase error	< 5 degree
Attenuation parameter (τ)	0.53 ± 0.02
Fill time	300 ns
Cell Q factor	$>10\,000$
Average shunt impedance	54 MΩ/m
Straightness	$< \pm 0.2$ mm
HOM damper	SiC absorber + choke structure
Choke frequency	5712 ± 11 MHz
Coupler type	*J*-type double feed

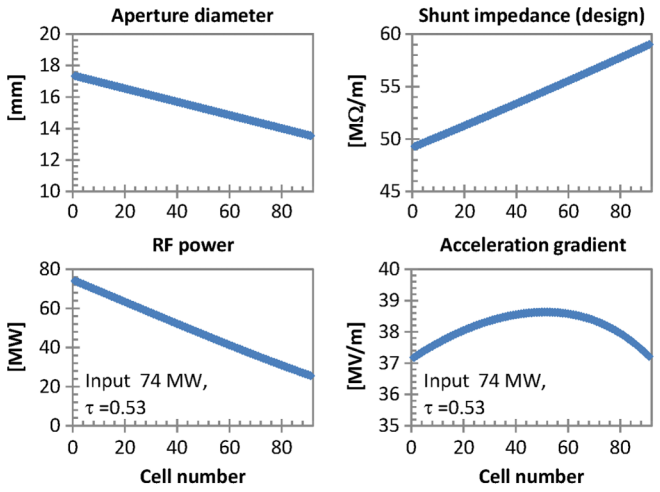

FIG. 5. Parameters of each accelerator cell; aperture diameter, designed shunt impedance and the computed rf power and acceleration gradient with an input power of 74 MW, which yields an average acceleration gradient of 38 MV/m.

Since 2006, 128 accelerator structures for SACLA were manufactured with the required accuracy. The rf amplitude and phase distribution were measured by the bead-pull method. The measured cell frequencies of the $3\pi/4$ mode were within ± 0.2 MHz. The integrated phase errors were kept within 2 degrees. The quality factors of the individual cells were higher than 10 000. The straightness of the structures was about 0.1 mm, better than the 0.3 mm requirement. Since the kick angle due to the wakefield is inversely proportional to the beam energy, we chose the better structures, such as those with relatively good straightness, for installation in the low-energy part of the SACLA accelerator.

E. rf pulse compression (SLED)

Figure 6 shows an outer view of the SLED-type rf pulse compressor for the *C*-band accelerator unit. Table II summarizes the SLED's parameters. The SLED system consists of a pair of $TE_{0,1,15}$ mode cavities and a 3-dB hybrid waveguide coupler. The cavity has a high Q factor because of the low-loss TE mode, which has no surface electric fields. At the entrance of each cavity, an rf mode converter is attached to convert the waveguide mode from rectangular TE10 to circular TE01. The rf mode converter uses a four-hole coupling, which symmetrically excites TE0x modes and reduces TE1x mode coupling. It also reduces the rf field around the edges of the coupling holes, which lowers the risk of rf breakdown. At the other end of the cavity, a frequency tuner with a differential screw is attached. This enables us to adjust the frequency to 5712 ± 0.02 MHz, which is required to maximize the rf compression gain, and to minimize any rf reflection to the klystron.

TABLE II. SLED parameters.

Resonant frequency	5712 ± 0.02 MHz
Resonant mode	TE0,1,15 (cylindrical)
Unloaded Q-factor	185 000
Coupling constant β	9.0
VSWR	<1.1
Power gain (average over 300 ns)	4

During operation, the rf power from the klystron builds up in the SLED cavities for the first 2 μs. Then the rf phase is changed by 180 degrees, which effectively discharges the stored rf energy. Figure 7 shows the theoretical rf power gain as a function of the coupling constant of the cavity. A large coupling constant gives a high power gain, although a higher peak power as well, which increases the risk of rf breakdown. We chose a coupling constant of 9 where the effective power gain levels off while the peak power continues to increase with larger coupling.

Sixty-four sets of the SLED cavities were carefully manufactured for SACLA. The resonant cavities, mode converters and 3-dB hybrid couplers were made of

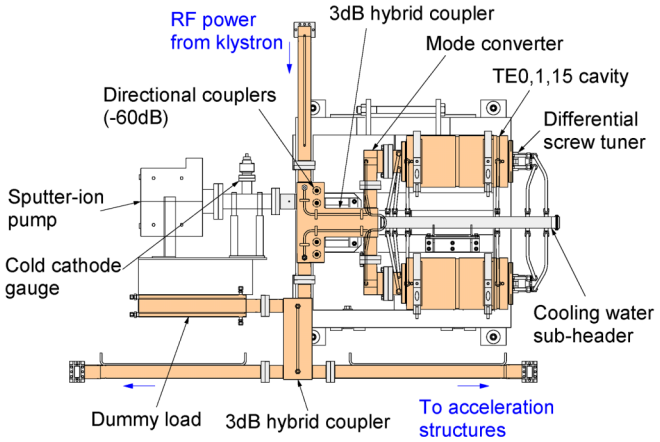

FIG. 6. Schematic of the SLED and surrounding waveguide and vacuum components.

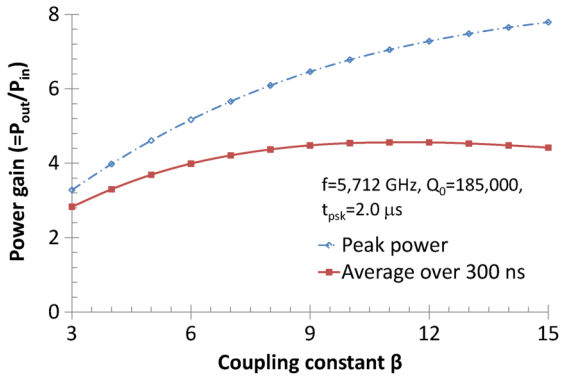

FIG. 7. Theoretical rf power gain as a function of the coupling constant of SLED. The structure gradient increases as the square root of the power gain averaged over 300 ns, the structure fill time.

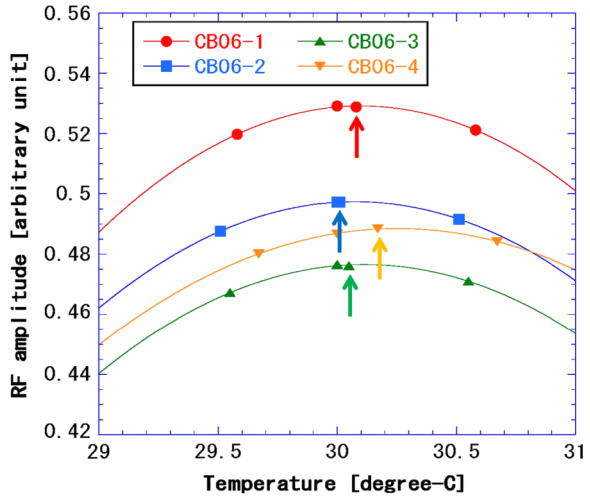

FIG. 8. Amplitudes of the SLED outputs as a function of the cavity temperature in four sets of *C*-band accelerator units: CB06-1, CB06-2, CB06-3 and CB06-4. The lines are a quadratic curve fit. The arrows represent the optimum temperature point.

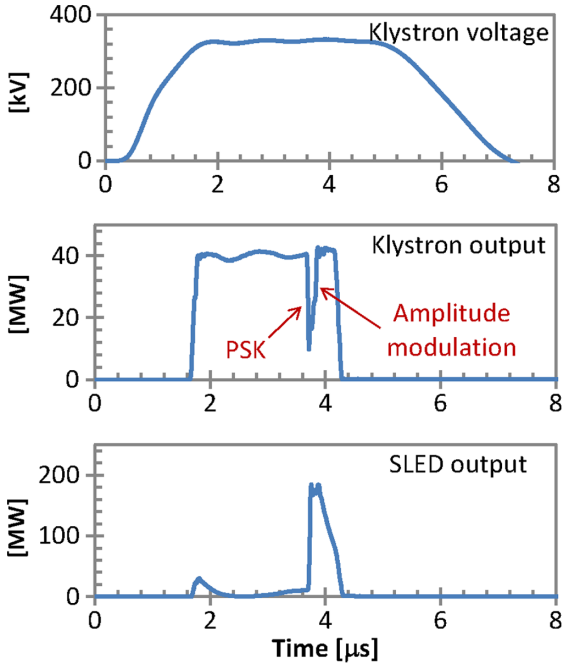

FIG. 9. Typical waveforms of the klystron cathode voltage, klystron output power and SLED output power for a 38 MV/m structure gradient. The phase switch keying (PSK) and the amplitude modulation applied by the LLRF system are also shown in the plot (see text).

high-purity, oxygen-free copper, and were assembled with a brazing method. After assembling a SLED system, its rf properties, such as the resonant frequency, Q factor and the coupling constant, were verified with a network analyzer. The cavity tuners were adjusted to set the resonant frequency within ± 20 kHz and to reduce the reflected voltage standing wave ratio (VSWR) to less than 1.1.

During high-power operation of the SLED, the resonant frequencies of the cavities were adjusted by changing the cooling water temperature. Figure 8 shows the output rf amplitude of four SLED systems as a function of the cavity temperature. The cavity temperature is regulated to ± 0.02 C around the optimum temperature in order to keep the output amplitude constant to within 0.1%.

Figure 9 shows the typical waveforms for the high voltage applied to the klystron, and the klystron and SLED output power. The high voltage pulse has a FWHM width of 4.5 μs to obtain a flattop of 3 μs. The pulse width of the klystron output is 2.5 μs, with phase switch keying (PSK) at 2.0 μs to discharge the cavity. The SLED output waveform spikes just after the PSK due to the natural rf power decay from the cavities. However, this spiky portion may cause rf breakdown, so it is reduced while keeping energy gain integrated over the 300 ns fill time of the accelerator structures constant. To do this, we applied amplitude modulation with the LLRF system to flatten the SLED's output pulse as shown in Fig. 9. The amplitude modulation effectively reduces the peak power of the spiky part from 250 to 200 MW, while the power amplification factor is slightly reduced to be 4.

F. Compact klystron modulator

Figures 10 and 11 show the circuit diagram and the interior view of the compact, oil-filled modulator. All of the high-voltage components, including a pulse-forming network (PFN) circuit with 16 capacitances and 16 inductors in series, a thyratron tube, a pulse transformer, and reverse current clipper circuits, are installed in a single steel tank filled with oil for electrical insulation. This design provides a reduction in size due to the superior insulation property of the oil, good EM noise-shield performance, and superior operational stability against environmental temperature and humidity variations.

We employed a conventional line-type modulator to achieve good reliability as the technology for this modulator approach is well established. Table III summarizes the specification of the modulator. As a high-voltage and high-current switch, we employed a thyratron, which has a fast switching time for the 5 kA primary current and a time jitter of less than 1 ns. It is also robust against a surge current due to a high-voltage discharge in the klystron. The 50 kV charging voltage and 1:16 winding ratio of the pulse transformer were determined based on the specifications of available thyratrons as well as the high-voltage and impedance requirements of the klystron. The PFN circuit has a capacitance of 29.3 nF and an inductance of 700 nH in 16 cells in order achieve a pulse width of 4.5 μs. The impedance of the PFN circuit, $Z_{pfn} = \sqrt{L/C} \sim 4.9\ \Omega$, matches the impedance of the klystron, $Z_L/n^2 \sim 4.3\ \Omega$. Three diodes are used for a EOL clipper, a tail clipper and a shunt circuit pass through for the reverse current, which reduces the voltage oscillation after the PFN is discharged.

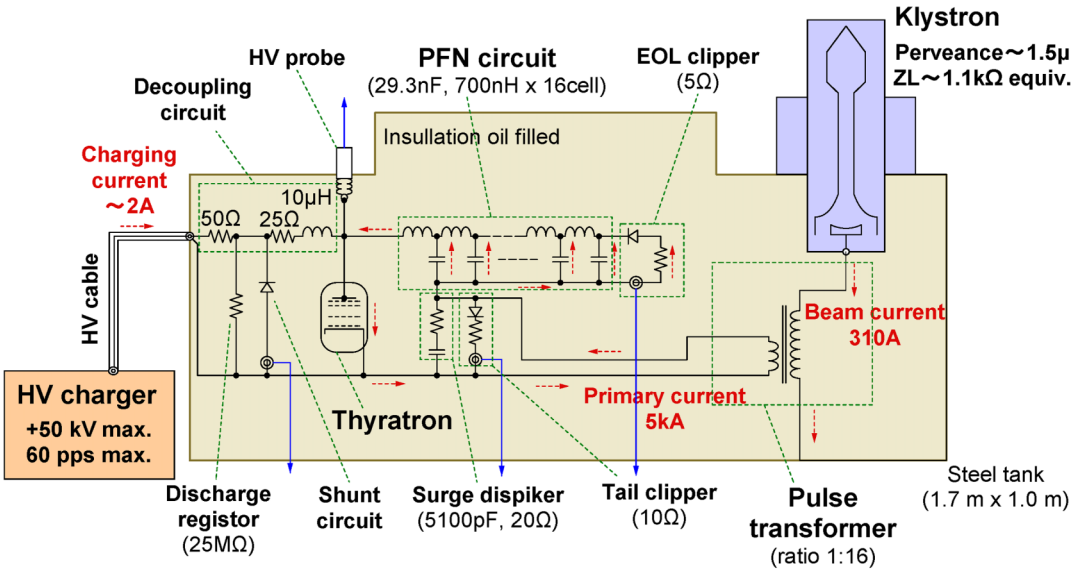

FIG. 10. Schematic of the klystron modulator. Typical charging current, primary pulse current and the secondary current for nominal operation are listed in the figure.

For the purpose of charging the PFN capacitors, we employ an inverter-type high-voltage charger. Due to a fast switching frequency of 20 kHz, the step-up transformers for typical inverters are quite small compared to that of 60 Hz transformers and inductors. However, commercial inverter-type high-voltage chargers have a certain amount of a residual voltage jitter, on the order of 0.1%. This voltage jitter would be the largest source of pulse-to-pulse amplitude and phase variations of the rf field. In order to suppress the jitter to less than 0.01% and stabilize the rf field within the tolerances, we have developed a special high-voltage charger, shown in Fig. 12 and Table IV. It has two charging circuits: the main charger and a subcharger, connected in parallel. The main charger is a coarse voltage control switching module with a relatively high power capacity using a full-bridge connection of insulated gate bipolar-transistors (IGBTs), a LC resonator, a step-up transformer and high-voltage rectifiers. It generates a charging current of 2 A, and quickly charges the PFN capacitors until 99.7% of the target voltage is reached in about 12 ms. Then, the subcharger starts to fill the PFN to achieve the target value. The subcharger has a relatively low-power capacity and uses a higher switching frequency than the main charger. In this case, field-effect transistors (FETs) are used as the switch devices. The switching voltage is regulated by a voltage dropper FET, which is

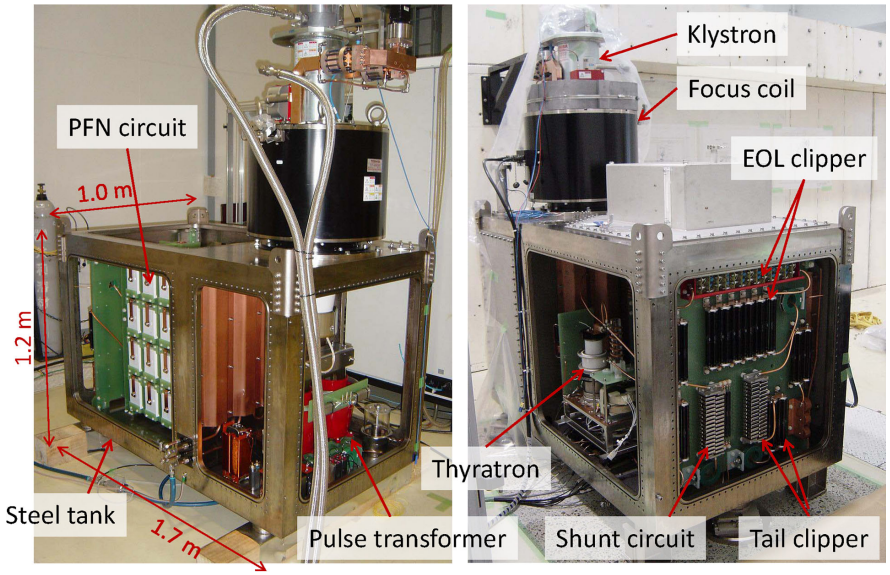

FIG. 11. Interior view of the klystron modulator.

TABLE III. Specifications of the klystron modulator.

Maximum charging voltage	50 kV
PFN circuit capacitance	470 nF
Pulse width (FWHM)	4.5 μs
Flattop width	3.0 μs
Rated output voltage	−350 kV
Rated output peak power	110 MW
Maximum repetition	60 pps
Size	1.7 m × 1 m × 1.2 m
High-voltage insulation	Mineral insulating oil (IEC 60296 transformer oil)

feedback controlled from the charging voltage signal. The charging voltage is measured by a temperature stabilized high-voltage probe attached to the PFN circuit. In order to reduce drift of the dividing ratio of the probe, the probe uses a precision resistor with a low temperature coefficient of $\pm 0.001\%/\mathrm{C}$. Its temperature is stabilized by cooling water through a Fluorinert medium.

Figure 13 shows a typical modulator charging waveform. The stability of the charging voltage is precisely analyzed using a high-resolution oscilloscope through a differential amplifier. The short-term voltage jitter was measured to be about 0.001% rms. This voltage jitter causes rf-field amplitude and phase fluctuations of only 0.0013% and 0.005 degrees in the accelerator structures, respectively.

III. OPERATION OF THE HIGH-GRADIENT ACCELERATOR

A. High power rf tests

The high-power performance of the above-mentioned rf components was investigated in a series of rf tests. Stable operation was realized after a period of rf conditioning. During this processing, the klystron rf power was gradually increased and resulted in small rf discharges that effectively cleaned the accelerator structures, waveguides and SLED inner surfaces. It also reduced the number of rf breakdowns. We performed rf conditioning using the following procedure: (i) Using an rf pulse shorter than 0.1 μs, the rf power was gradually increased from several MW to about 45 MW, while maintaining a vacuum pressure below the threshold value of 1×10^{-5} Pa. (ii) Once the power reached the target value (typically 45 MW), the pulse width was gradually expanded from 0.2 μs to 1.0 μs. (iii) The pulse width was then increased from 1.0 μs to 2.5 μs, during which the PSK operation was applied to achieve rf pulse compression. (iv) After the pulse width was expanded to the nominal value of 2.5 μs, the conditioning operation was continued at an rf power of 45 MW or more. Long-term operation further reduced the trip rate.

The first high-power test of an accelerator structure was performed in 2004. Without using SLED, rf power of up to 55 MW from the klystron was fed directly into one accelerator structure. After rf conditioning for 300 hours, a gradient of 33 MV/m was achieved without any serious problems. The SLED system was independently tested at KEK. The high-power rf performance of SLED was tested up to an rf output power of 135 MW [21]. In 2005, two *C*-band accelerator units including SLED were installed at the prototype free-electron laser facility called the SCSS test accelerator [22], as a demonstration of the FEL and the operational performance of accelerator components. The *C*-band accelerator units were initially operated at an

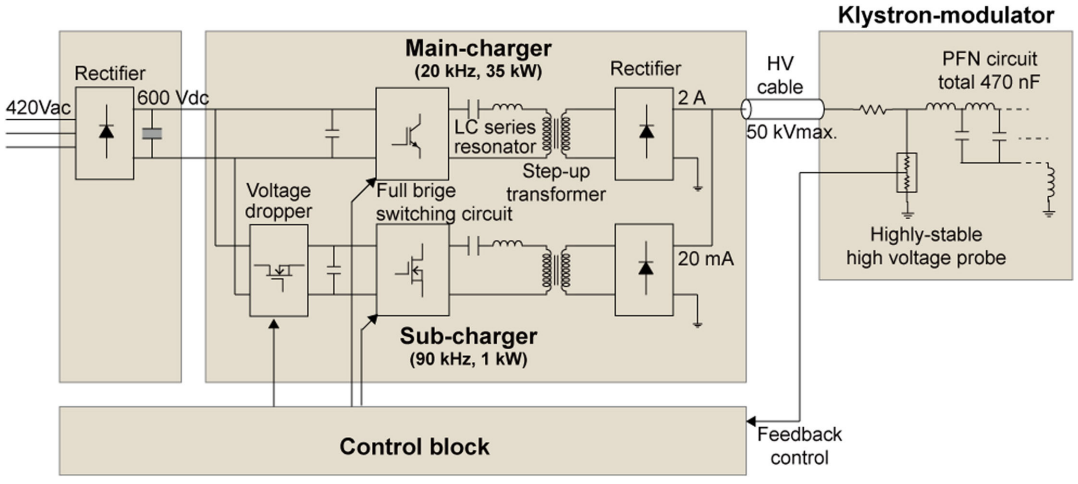

FIG. 12. Schematic of the high-voltage charger. It has two charging circuits: a main charger and a subcharger, connected in parallel.

TABLE IV. Specifications of the high-voltage charger.

Maximum charging voltage	50 kV
Charging current	Main charger: 2 A Sub charger: 20 mA
Maximum output power	36 kW
Maximum repetition	60 pps
Power efficiency	87% (50 kV, 60 pps)
Power factor	87% (50 kV, 60 pps)
rms charging voltage stability	0.001% pulse to pulse, 0.03% long term
Size	19 inch rack mount, 0.4 m × 0.6 m × 1.4 m

acceleration gradient of 29 MV/m in order to accelerate electron beams up to 250 MeV. Besides the accelerator operation, we rf conditioned the structures for 500 hours to obtain a high gradient with a low trip rate. As a result, we raised the acceleration gradient to 37 MV/m for daily operation [23]. These results proved that there are no technical problems with running the structures at high gradient. After this test operation at the SCSS test accelerator, we started mass production of the *C*-band accelerator components for SACLA construction.

In order to check the quality of the mass-produced components, high-power rf tests were performed at the test stand. One *C*-band accelerator unit, including the vacuum system, cooling water system, LLRF system and control system, were installed using the nominal layout and cabling. After 450 hours of high-power rf conditioning, we obtained a gradient of more than 40 MV/m in the accelerator structures. Figure 14 shows the trip rates due to rf breakdown, which is identified by the significant power reflection to the klystron that it causes. At 38 MV/m, the trip rate was less than once per day with a pulse rate of 60 pps, which meets the SACLA requirements. At 39 MV/m, the trip rate was 6 times per day after 200 hours of conditioning. After an additional 200 hours of conditioning, the trip rate decreased significantly, to once per day. We confirmed that the performance of the rf components was sufficient to operate at over 38 MV/m in SACLA based on these results.

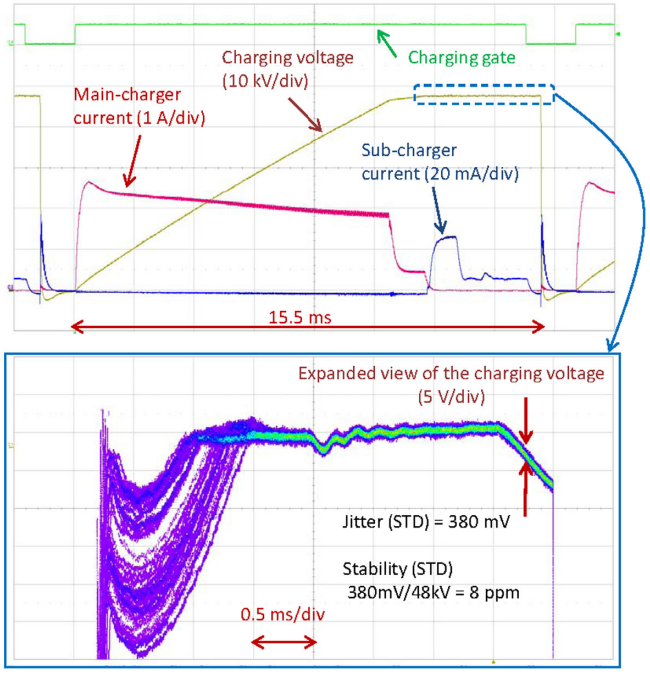

FIG. 13. Typical waveform during the PFN charging sequence. The bottom figure shows the expanded flat part of the charging voltage where 20 waveforms are overlaid to indicate the voltage stability.

B. Operational performance at SACLA and discussion

The SACLA accelerator was constructed in 2009 and 2010. After installation of the rf components described above, various tasks were done to complete the system: alignment, cabling, cooling water connections, control system setup, and finally high-power rf conditioning. The rf conditioning required roughly 1000 hours operation at the design acceleration gradient of 35 MV/m to achieve an acceptable trip rate of once per day with a 10 pps repetition rate. In February 2011, XFEL commissioning was started with a lower than nominal beam energy of 7 GeV. During the night shifts we performed additional rf conditioning in order to increase the gradient up to 38 MV/m to obtain a beam energy of 8 GeV.

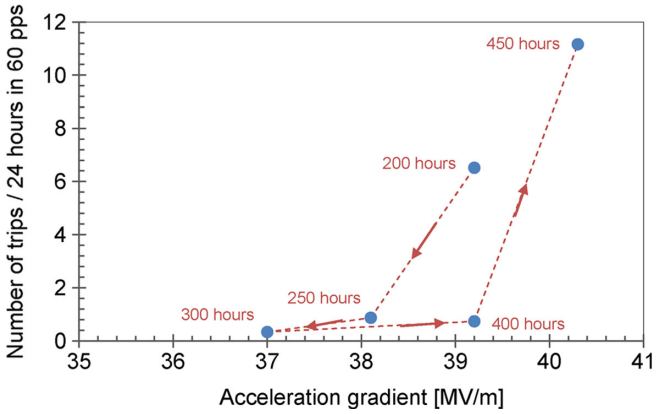

FIG. 14. Record of the trip rates during high-power rf conditioning at the test stand.

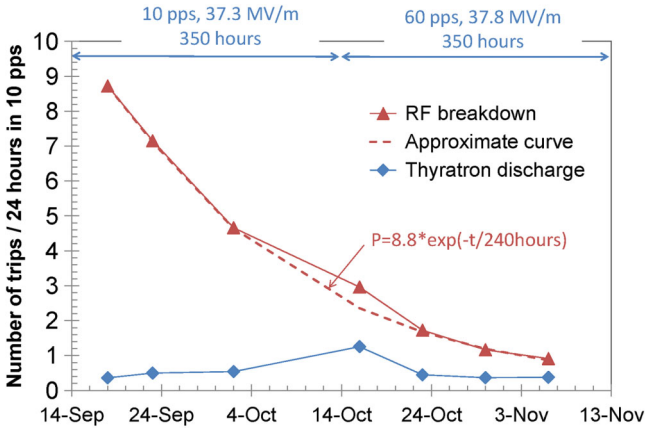

FIG. 15. Variation of the trip rate caused by rf breakdowns (red triangle) and early discharges of the thyratron (blue circle) during rf conditioning. The dashed line is an exponential fit to the rf breakdown trip rate.

Figure 15 shows how the trip rate changed over time, decreasing roughly exponentially with a 240 hour time constant. After conditioning for 700 hours, the rf breakdown rate had decreased by a factor of 10, which allowed operation up to a beam energy of 8.5 GeV to produce up to 20 keV photons. The pulse repetition rate of the SACLA accelerator was initially set at 10 pps. After trip rate decreased, the repetition rate was increased to 30 pps in 2013. So far, the 64 *C*-band accelerator units have been operated for about 20 000 hours, without any serious high-power rf component problems.

Figure 16 shows the acceleration gradient of the individual *C*-band accelerator units for two sets of typical beam energies. The averaged acceleration gradients are set at 38 and 35 MV/m for the electron beam energies of 8.5 and 7.9 GeV, respectively. The electron beam energy was measured in the magnetic chicanes just upstream of the undulators. The beam energy was also estimated from the photon energy of the undulator radiation. The acceleration gradient of each unit was calibrated by measuring the energy difference with and without the accelerator unit on. These measurements agree well with the values estimated from the rf power measured upstream of the accelerator structures, within an error of 10%.

A typical trip rate when running at 8 GeV, 30 pps is about once per day for each unit, and once per 20 minutes for the whole SACLA accelerator. This trip rate is considered acceptable for the current user experiments. Roughly half of the trips are caused by the prefiring of the thyratrons and about 5%–10% of the trips are caused by arcing in the klystrons; the other trips are caused by rf breakdown in the accelerator structures.

A prefire of the thyratron without any trigger pulses is an event that discharges the PFN during the nominal charging period. Formerly, the interlock system detected an insufficient charging voltage and halted the next charging. Since most discharges occurred accidentally and did not affect to the next pulse, we modified the interlock sequence so as not to halt operation if a single discharge event occurred. The reduced the thyratron-related trip rate by two-thirds and there was no damage to the thyratrons.

Radio-frequency breakdown is still a major source of accelerator trips, especially for operation above 37 MV/m. To investigate the possibility of running at a higher electron beam energy to extend the x-ray energy range, we tentatively increased the gradient to 40 MV/m. Figure 17 shows how the average trip rate changed with gradient. We found that the rf breakdown rate is roughly proportional to the 30th power of the acceleration gradient (dashed line in Fig. 17). We gradually raised the gradient in a step-by-step manner, and after operating for 116 hours, the gradient was set back to 37.8 MV/m, where the trip rate decreased to 70% of initial rate at this gradient. We expect that with further rf conditioning, the trip rate will continue to

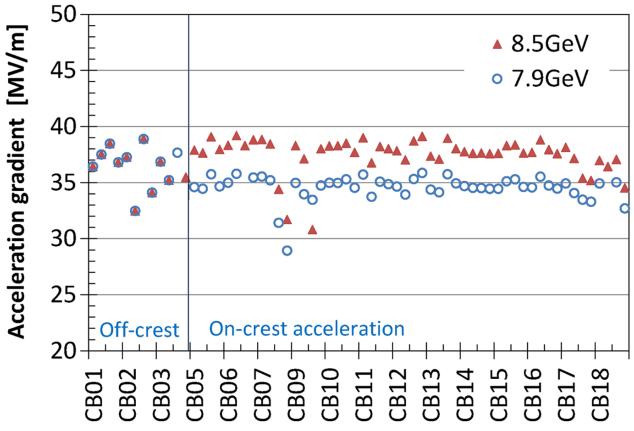

FIG. 16. Typical acceleration gradients versus *C*-band unit number for 8.5 GeV (red triangle) and 7.9 GeV (blue circle) operation. The variation of the gradient is just the individual difference of the klystron output power.

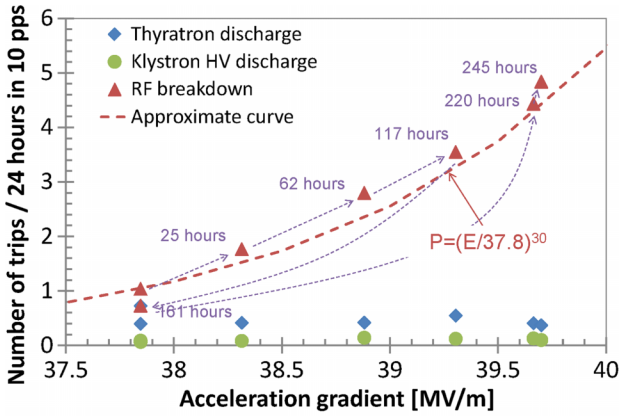

FIG. 17. Average trip rate of the *C*-band accelerator units as a function of gradient. The number of hours operated during each measurement are also shown.

TABLE V. Typical pulse-to-pulse rms stabilities. The values in brackets are the measurement errors, estimated by the fluctuations with no signal.

Modulator charging voltage	0.0007% (0.0007%)
Klystron cathode voltage	0.0024% (0.0016%)
Klystron beam current	0.0025% (0.0018%)
Klystron rf amplitude	0.0092% (0.0075%)
Klystron rf phase	0.03 degree

decrease, which will enable us to increase the electron beam energy.

Dark current from the accelerator structures was measured by current transformers [13] installed between the *C*-band accelerator units. The total amount of dark current was less than 5 pC per pulse per unit for an 8 GeV electron beam energy. This dark current level is about 1 order of magnitude smaller than the electron bunch charge, and has a negligible effect on the beam monitors.

The pulse-to-pulse stability of the PFN voltage, klystron voltage, rf amplitude and phase of the klystron output were measured, and are summarized in Table V (note many of these values are limited by the resolutions of the measurement instruments). Thanks to precise regulation of the PFN voltage, the rf amplitude and phase were within the 0.01% and 0.2 degree rms tolerances demanded by the XFEL operation The drift of the rf phase is corrected by the LLRF feedback system. In addition, drifts of the electron beam energy and trajectory due to the gradient variations are compensated by several beam-based feedback loops. The stability of the final electron beam energy is consequently 0.02% rms pulse to pulse, and 0.03% peak to peak for long-term drift. These values are smaller than the 0.1% energy spread of the electron beam and the 0.3% FWHM spectral band width of the x rays. The pulse-to-pulse variation of the beam energy at the final bunch compressor BC3 is about 0.05%–0.1% rms, which gives acceptable bunch compression stability for usual XFEL operation. Therefore, the *C*-band accelerators have a sufficient gradient stability for producing photons for user experiments.

Although the accelerator structures have wakefield damping built into every cell, multibunched beam operation has not yet been tested. However, it will be tested for a future upgrade of SACLA.

IV. SUMMARY

C-band (5.712 GHz) accelerator units have been successfully developed for SACLA linac. The accelerator structures and pulse compressors were carefully designed, fabricated, tested and installed in the SACLA accelerator tunnel. After an rf conditioning time of 1700 hours, the *C*-band linac runs stably at a gradient as high as 38 MV/m, accelerating an electron beam up to 8.5 GeV. The accelerator trip rate of SACLA is about once per 20 minutes at a 30 pps repetition rate, which is acceptable for user experiments. The amount of dark current from an accelerator structure is less than 5 pC per pulse, which produces an acceptably low background noise level in the beam monitors.

A compact oil-filled modulator, combined with an extremely stable inverter-type high-voltage charger was developed. The size of the modulator is 1.7 m × 1 m, which was installed within the 4 m accelerator unit period length in the klystron gallery. The pulse-to-pulse stability of the charging voltage of the modulator is less than 10 ppm rms. The stability of the accelerator rf amplitude and phase is less than 100 ppm and 0.03 degree, which enables us to realize stable acceleration and bunch compression of the electron beam.

The operational performance of the high-gradient *C*-band linac has been demonstrated in SACLA. The excellent qualities of compactness, efficiency, and stability are important for linac-based light sources, such as XFELs and seeded FELs. The high gradient *C*-band linac is also applicable to a linear collider to shorten the total length of the linac. The technology and rf components for the *C*-band frequency can also be applied to small industrial linacs, and injectors used in low-emittance storage rings.

ACKNOWLEDGMENTS

The authors give thanks to all staff members of SACLA and SPring-8 for their continuous support, especially Dr. T. Ishikawa, Dr. N. Kumagai, and Dr. H. Tanaka for their management and promotion. The authors also thank Professor H. Matsumoto, Professor H. Baba, Dr. M. Yoshida, and Mr. N. Akasaka, belonging to JLC *C*-band design team in the past, for developing the basic components. The authors also give thanks to Dr. S. Miura of Mutsubishi Heavy Industries Ltd., Mr. Y. Ohkubo of Toshiba Electron Tubes & Devices Co., Ltd., Dr. A. Tokuchi of Nichicon Corp., and Mr. K. Sato of Nohon Koshuha Co., Ltd., for practical engineering work and execution of production with excellent quality.

[1] P. Emma *et al.*, Nat. Photonics **4**, 641 (2010).
[2] R. B. Neal *et al.*, *The Stanford Two-Mile Accelerator* (W. A. Benjamin, New York, 1968).
[3] Z. D. Farkas *et al.*, Report No. SLAC-PUB-1453, 1974.
[4] T. Shintake *et al.*, in *Proceedings of the Particle Accelerator Conference, Dallas, TX, 1995* (IEEE, New York, 1995).
[5] JLC group, KEK Report No. 92-16, 1992; C. Adolphsen *et al.*, SLAC Report No. 474, 1996.
[6] D. Pritzkau, and R. Siemann, Phys. Rev. ST Accel. Beams **5**, 112002 (2002).
[7] K. Bane, Report No. SLAC-PUB-9663, 2003.
[8] T. Shintake *et al.*, in *Proceedings of the Particle Accelerator Conference, Vancouver, BC, Canada, 1997* (IEEE, New York, 1997).

[9] T. Shintake, H. Matsumoto, T. Ishikawa, and H. Kitamura, Proc. SPIE Int. Soc. Opt. Eng. **4500**, 12 (2001).
[10] T. Ishikawa *et al.*, Nat. Photonics **6**, 540 (2012).
[11] K. Togawa, T. Shintake, T. Inagaki, K. Onoe, T. Tanaka, H. Baba, and H. Matsumoto, Phys. Rev. ST Accel. Beams **10**, 020703 (2007).
[12] K. Togawa, T. Hara, and H. Tanaka, Phys. Rev. ST Accel. Beams **12**, 080706 (2009)
[13] Y. Otake, H. Maesaka, S. Matsubara, S. Inoue, K. Yanagida, H. Ego, C. Kondo, T. Sakurai, T. Matsumoto, and H. Tomizawa, Phys. Rev. ST Accel. Beams **16**, 042802 (2013).
[14] H. Maesaka *et al.*, in *Proceedings of the 12th International Conference on Accelerator and Large Experimental Physics Control Systems, Kobe, Japan* (SPring-8, Japan, 2009).
[15] T. Hasegawa *et al.*, in *Proceedings of the International Particle Accelerator Conference, Kyoto, Japan* (ICR, Kyoto, 2010).
[16] R. Tanaka *et al.*, in *Proceedings of the 6th International Conference on Accelerator and Large Experimental Physics Control Systems, Beijing, China* (IHEP, China, 1997).
[17] T. Shintake, Jpn. J. Appl. Phys. **31**, L1567 (1992); in *Proceedings of the 18th Particle Accelerator Conference, New York, 1999* (IEEE, New York, 1999).
[18] C. Suzuki *et al.*, in *Proceedings of the Particle Accelerator Conference, Vancouver, BC, Canada, 1997* (Ref. [8]).
[19] H. Maesaka *et al.*, in *Proceedings of the 35th International Free-Electron Laser Conference, New York* (BNL, New York, 2013).
[20] H. Matsumoto *et al.*, in *Proceedings of 18th International Linac Conference, Geneva, Switzerland* (CERN, Geneva, Switzerland, 1996).
[21] M. Yoshida, Ph.D. thesis, University of Tokyo, 2003.
[22] T. Shintake *et al.*, Phys. Rev. ST Accel. Beams **12**, 070701 (2009).
[23] T. Inagaki *et al.*, in *Proceedings of 24th Linear Accelerator Conference, Victoria, Canada* (TRIUMF, Canada, 2008).